J|A|C|S ARTICLES

Published on Web 12/15/2009

Zn^{2+}-Triggered Amide Tautomerization Produces a Highly Zn^{2+}-Selective, Cell-Permeable, and Ratiometric Fluorescent Sensor

Zhaochao Xu,*[,†,‡] Kyung-Hwa Baek,[§] Ha Na Kim,[†] Jingnan Cui,[||] Xuhong Qian,[⊥] David R. Spring,[‡] Injae Shin,*[,§] and Juyoung Yoon*[,†]

Department of Chemistry and Nano Science and Department of Bioinspired Science, Ewha Womans University, Seoul 120-750, Korea, Department of Chemistry, University of Cambridge, Cambridge, CB2 1EW, United Kingdom, Department of Chemistry, Yonsei University, Seoul 120-749, Korea, State Key Laboratory of Fine Chemicals, Dalian University of Technology, Dalian 116012, China, and Shanghai Key Laboratory of Chemical Biology, East China University of Science and Technology, Shanghai 200237, China

Received August 30, 2009; E-mail: zx214@cam.ac.uk; injae@yonsei.ac.kr; jyoon@ewha.ac.kr

Abstract: It is still a significant challenge to develop a Zn^{2+}-selective fluorescent sensor with the ability to exclude the interference of some heavy and transition metal (HTM) ions such as Fe^{2+}, Co^{2+}, Ni^{2+}, Cu^{2+}, Cd^{2+}, and Hg^{2+}. Herein, we report a novel amide-containing receptor for Zn^{2+}, combined with a naphthalimide fluorophore, termed **ZTRS**. The fluorescence, absorption detection, NMR, and IR studies indicated that **ZTRS** bound Zn^{2+} in an imidic acid tautomeric form of the amide/di-2-picolylamine receptor in aqueous solution, while most other HTM ions were bound to the sensor in an amide tautomeric form. Due to this differential binding mode, **ZTRS** showed excellent selectivity for Zn^{2+} over most competitive HTM ions with an enhanced fluorescence (22-fold) as well as a red-shift in emission from 483 to 514 nm. Interestingly, the **ZTRS**/Cd^{2+} complex showed an enhanced (21-fold) blue-shift in emission from 483 to 446 nm. Therefore, **ZTRS** discriminated in vitro and in vivo Zn^{2+} and Cd^{2+} with green and blue fluorescence, respectively. Due to the stronger affinity, Zn^{2+} could be ratiometrically detected in vitro and in vivo with a large emission wavelength shift from 446 to 514 nm via a Cd^{2+} displacement approach. **ZTRS** was also successfully used to image intracellular Zn^{2+} ions in the presence of iron ions. Finally, we applied **ZTRS** to detect zinc ions during the development of living zebrafish embryos.

Introduction

Fluorescent sensors are powerful tools to monitor in vitro and/or in vivo biologically relevant species such as metal ions because of the simplicity and high sensitivity of fluorescence.[1] A typical fluorescent sensor contains a receptor (the recognition site) linked to a fluorophore (the signal source) which translates the recognition event into the fluorescence signal.[2] Therefore, an ideal fluorescent sensor must meet two basic requirements. First, the receptor must have the strongest affinity with species of interest (binding selectivity), which is the central processing unit of a sensor. Second, the fluorescence signal should not be perturbed by the environment (signal selectivity). Most reported fluorescent sensors display an increase or decrease in the emission intensity upon binding to species of interest. However, ratiometric responses are more attractive because the ratio between the two emission intensities can be used to measure the analyte concentration and provide a built-in correction for environmental effects, such as photobleaching, sensor molecule concentration, the environment around the sensor molecule (pH, polarity, temperature, and so forth), and stability under illumination.[3]

Optical imaging with fluorescent sensors for Zn^{2+} has attracted great attention, owing to the biological significance of zinc.[4] Zinc is the second most abundant transition metal ion in the human body after iron, and is an essential cofactor in many biological processes such as brain function and pathology, gene transcription, immune function, and mammalian repro-

[†] Ewha Womans University.
[‡] University of Cambridge.
[§] Yonsei University.
[||] Dalian University of Technology.
[⊥] East China University of Science and Technology.

(1) Tsien, R. Y. In *Fluorescent and Photochemical Probes of Dynamic Biochemical Signals inside Living Cells*; Czarnik, A. W., Ed.; American Chemical Society: Washington, DC, 1993; pp 130−146.
(2) (a) Callan, J. F.; de Silva, A. P.; Magri, D. C. *Tetrahedron* **2005**, *61*, 8551–8588. (b) Rurack, K. *Spectrochim. Acta Part A* **2001**, *57*, 2161–2195. (c) Czarnik, A. W. *Acc. Chem. Res.* **1994**, *27*, 302–308. (d) Valeur, B.; Leray, I. *Coord. Chem. Rev.* **2000**, *205*, 3–40. (e) Prodi, L.; Bolletta, F.; Montalti, M.; Zaccheroni, N. *Coord. Chem. Rev.* **2000**, *205*, 59–83. (f) Kim, H.; Lee, M.; Kim, H.; Kim, J.; Yoon, J. *Chem. Soc. Rev.* **2008**, *37*, 1465–1472.
(3) (a) Grynkiewicz, G.; Poenie, M.; Tsien, R. Y. *J. Biol. Chem.* **1985**, *260*, 3440–3450. (b) Xu, Z.; Xiao, Y.; Qian, X.; Cui, J.; Cui, D. *Org. Lett.* **2005**, *7*, 889–892.
(4) Recent reviews for zinc sensors: (a) Que, E. L.; Domaille, D. W.; Chang, C. *J. Chem. Rev.* **2008**, *108*, 1517–1549. (b) Nolan, E. M.; Lippard, S. *J. Acc. Chem. Res.* **2009**, *42*, 193–203. (c) Dai, Z.; Canary, J. W. *New J. Chem.* **2007**, *31*, 1708–1718. (d) Jiang, P.; Guo, J. *Coord. Chem. Rev.* **2004**, *248*, 205–229. (e) Carol, P.; Sreejith, S.; Ajayaghosh, A. *Chem. Asian J.* **2007**, *2*, 338–348. (f) Lim, N. C.; Freake, H. C.; Bru'ckner, C. *Chem.—Eur. J.* **2005**, *11*, 38–49. (g) Kimura, E.; Aoki, S. *Biometals* **2001**, *14*, 191–204. (h) Domaille, D. W.; Que, E. L.; Chang, C. *J. Nat. Chem. Biol.* **2008**, *4*, 168–175.

duction.[5,6] This ion is also involved in pathological processes, such as Alzheimer's disease, epilepsy, ischemic stroke, and infantile diarrhea.[7−9] Although most biological zinc ions are tightly bound to proteins (playing structural and catalytic roles), loosely bound or chelatable zinc, which are the main target of fluorescent sensors, are present in various human tissues, including the brain,[10] intestine,[11] pancreas,[12] and retina.[13] Up to now, a variety of fluorescent sensors for Zn^{2+} have been developed with some successful applications to image Zn^{2+} in living cells or hippocampus slices,[14−16] perhaps most notably by Lippard[15] and Nagano.[16] Recently, Guo et al. reported a fluorescent sensor to trace intact Zn^{2+} in zebrafish embryos.[17] However, only a few ratiometric fluorescent sensors for Zn^{2+} have been reported.[18] Additionally, to our best knowledge, all these reported sensors have a shortcoming in that they suffer from interference of some heavy and transition metal (HTM) ions such as Fe^{2+}, Co^{2+}, Ni^{2+}, Cu^{2+}, and Hg^{2+}. Even though the reported sensors show a selective turn-on fluorescence signal for Zn^{2+}, they often display poor binding selectivity for Zn^{2+} over other HTM ions.[18h] Their low selectivity for Zn^{2+} may result from the use of di-2-picolylamine (DPA),[15,16,19] acyclic and cyclic polyamines,[20] iminodiacetic acid,[14d,21] bipyridine,[18e,22] quinoline,[23] and Schiff-bases[24] as Zn^{2+}-chelators, which have similar affinities to other HTM ions. In addition, some available Zn^{2+} sensors have difficulty in distinguishing Zn^{2+} and Cd^{2+}, since Cd^{2+} is in the same group of the periodic table and has similar properties with Zn^{2+}. Therefore, similar fluorescence changes including the change of intensity and the shift of wavelengths are usually observed when Zn^{2+} and Cd^{2+} are coordinated with fluorescent sensors. In recent years, Cui et al.[25a] and Jiang et al.[25b,c] reported sensors which can discriminate Zn^{2+} and Cd^{2+} with different emission wavelengths; however, these sensors have a stronger affinity for Cd^{2+}.

After the first attachment to fluorescein in 1996,[26] DPA has been used as the most popular receptor for Zn^{2+} sensors. Some DPA-derivatives, such as *N*,*N*-di-(2-picolyl)ethylenediamine (DPEN),[27] tris(2-pyridylmethyl)amine (TPA)[14c,28] and *N*,*N*,*N*′-tris(pyridin-2-ylmethyl)ethylenediamine (TRPEN),[17,29] were subsequently devised as Zn^{2+} chelators, because DPA-related chelators confer selectivity for Zn^{2+} over cations that occur in much higher concentrations in biological samples, such as Ca^{2+}, Mg^{2+}, K^+, and Na^+. Since these chelators can also bind other HTM ions strongly, new strategies should be exploited to improve the Zn^{2+} selectivity of receptors. One possible approach is to impose the conformational restraint to the chelator of ions

(5) Frederickson, C. J.; Koh, J.-Y.; Bush, A. I. *Nat. Rev. Neurosci.* **2005**, *6*, 449–462.
(6) Fraker, P. J.; King, L. E. *Annu. Rev. Nutr.* **2004**, *24*, 277–298.
(7) Bush, A. I.; Pettingell, W. H.; Multhaup, G.; Paradis, M.; Vonsattel, J.-P.; Gusella, J. F.; Beyreuther, K.; Masters, C. L.; Tanzi, R. E. *Science* **1994**, *265*, 1464–1467.
(8) Koh, J. Y.; Suh, S. W.; Gwag, B. J.; He, Y. Y.; Hsu, C. Y.; Choi, D. W. *Science* **1996**, *272*, 1013–1016.
(9) Walker, C. F.; Black, R. E. *Annu. Rev. Nutr.* **2004**, *24*, 255–275.
(10) Galasso, S. L.; Dyck, R. H. *Mol. Med.* **2007**, *13*, 380–387.
(11) Giblin, L. J.; Chang, C. J.; Bentley, A. F.; Frederickson, C.; Lippard, S. J.; Frederickson, C. J. *J. Histochem. Cytochem.* **2006**, *54*, 311–316.
(12) Dunn, M. F. *BioMetals* **2005**, *18*, 295–303.
(13) Redenti, S.; Ripps, H.; Chappell, R. L. *Exp. Eye Res.* **2007**, *85*, 580–584.
(14) (a) Frederickson, C. J.; Kasarskis, E. J.; Ringo, D.; Frederickson, R. E. *J. Neurosci. Methods* **1987**, *20*, 91–103. (b) Nasir, M. S.; Fahrni, C. J.; Suhy, D. A.; Kolodsick, K. J.; Singer, C. P.; O'Halloran, T. V. *J. Biol. Inorg. Chem.* **1999**, *4*, 775–783. (c) Sumalekshmy, S.; Henary, M. M.; Siegel, N.; Lawson, P. V.; Wu, Y.; Schmidt, K.; Brédas, J.-L.; Perry, J. W.; Fahrni, C. J. *J. Am. Chem. Soc.* **2007**, *129*, 11888–11889. (d) Sensi, S. L.; Ton-That, D.; Weiss, J. H.; Rothe, A.; Gee, K. R. *Cell Calcium* **2003**, *34*, 281–284.
(15) (a) Walkup, G. K.; Burdette, S. C.; Lippard, S. J.; Tsien, R. Y. *J. Am. Chem. Soc.* **2000**, *122*, 5644–5645. (b) Zhang, X.; Lovejoy, K. S.; Jasanoff, A.; Lippard, S. J. *Proc. Natl. Acad. Sci. U.S.A.* **2007**, *104*, 10780–10785. (c) Wong, B. A.; Friedle, S.; Lippard, S. J. *J. Am. Chem. Soc.* **2009**, *131*, 7142–7152. (d) Burdette, S. C.; Frederickson, C. J.; Bu, W.; Lippard, S. J. *J. Am. Chem. Soc.* **2003**, *125*, 1778–1787. (e) Zhang, X.; Hayes, D.; Smith, S. J.; Friedle, S.; Lippard, S. J. *J. Am. Chem. Soc.* **2008**, *130*, 15788–15789. (f) Tomat, E.; Nolan, E. M.; Jaworski, J.; Lippard, S. J. *J. Am. Chem. Soc.* **2008**, *130*, 15776–15777.
(16) (a) Hanaoka, K.; Kikuchi, K.; Kojima, H.; Urano, Y.; Nagano, T. *Angew. Chem., Int. Ed.* **2003**, *42*, 2996–2999. (b) Hirano, T.; Kikuchi, K.; Urano, Y.; Nagano, T. *J. Am. Chem. Soc.* **2002**, *124*, 6555–6562. (c) Hanaoka, K.; Kikuchi, K.; Kojima, H.; Urano, Y.; Nagano, T. *J. Am. Chem. Soc.* **2004**, *126*, 12470–12476.
(17) Qian, F.; Zhang, C.; Zhang, Y.; He, W.; Gao, X.; Hu, P.; Guo, Z. *J. Am. Chem. Soc.* **2009**, *131*, 1460–1468.
(18) (a) Xue, L.; Liu, C.; Jiang, H. *Chem. Commun.* **2009**, 1061–1063. (b) Maruyama, S.; Kikuchi, K.; Hirano, T.; Urano, Y.; Nagano, T. *J. Am. Chem. Soc.* **2002**, *124*, 10650–10651. (c) Woodroofe, C. C.; Lippard, S. J. *J. Am. Chem. Soc.* **2003**, *125*, 11458–11459. (d) Taki, M.; Wolford, J. L.; O'Halloran, T. V. *J. Am. Chem. Soc.* **2004**, *126*, 712–713. (e) Ajayaghosh, A.; Carol, P.; Sreejith, S. *J. Am. Chem. Soc.* **2005**, *127*, 14962–14963. (f) Kiyose, K.; Kojima, H.; Urano, Y.; Nagano, T. *J. Am. Chem. Soc.* **2006**, *128*, 6548–6549. (g) Chang, C. J.; Jaworski, J.; Nolan, E. M.; Sheng, M.; Lippard, S. J. *Proc. Natl. Acad. Sci. U.S.A* **2004**, *101*, 1129–1134. (h) Xu, Z.; Qian, X.; Cui, J.; Zhang, R. *Tetrahedron* **2006**, *62*, 10117–10122. (i) Komatsu, K.; Urano, Y.; Kojima, H.; Nagano, T. *J. Am. Chem. Soc.* **2007**, *129*, 13447–13454. (j) Henary, M. M.; Wu, Y.; Fahrni, C. J. *Chem.—Eur. J.* **2004**, *10*, 3015–3025.
(19) (a) Atilgan, S.; Ozdemir, T.; Akkaya, E. U. *Org. Lett.* **2008**, *10*, 4065–4067. (b) Huang, S.; Clark, R. J.; Zhu, L. *Org. Lett.* **2007**, *9*, 4999–5002. (c) Wu, Y.; Peng, X.; Guo, B.; Fan, J.; Zhang, Z.; Wang, J.; Cui, A.; Gao, Y. *Org. Biomol. Chem.* **2005**, *3*, 1387–1392. (d) Royzen, M.; Durandin, A.; Young, V. G., Jr.; Geacintov, N. E.; Canary, J. W. *J. Am. Chem. Soc.* **2006**, *128*, 3854–3855. (e) Tang, B.; Huang, H.; Xu, K.; Tong, L.; Yang, G.; Liu, X.; An, L. *Chem. Commun.* **2006**, 3609–3611. (f) Henary, M. M.; Wu, Y.; Fahrni, C. J. *Chem.—Eur. J.* **2004**, *10*, 3015–3025.
(20) (a) Tamanini, E.; Katewa, A.; Sedger, L. M.; Todd, M. H.; Watkinson, M. *Inorg. Chem.* **2009**, *48*, 319–324. (b) Aoki, S.; Sakurama, K.; Ohshima, R.; Matsuo, N.; Yamada, Y.; Takasawa, R.; Tanuma, S.; Takeda, K.; Kimura, E. *Inorg. Chem.* **2008**, *47*, 2747–2754. (c) Hirano, T.; Kikuchi, K.; Urano, Y.; Higuchi, T.; Nagano, T. *Angew. Chem., Int. Ed.* **2000**, *39*, 1052–1054.
(21) Major, J. L.; Parigi, G.; Luchinat, C.; Meade, T. J. *Proc. Natl. Acad. Sci. U.S.A* **2007**, *104*, 13881–13886.
(22) (a) Dennis, A. E.; Smith, R. C. *Chem. Commun.* **2007**, 4641–4643. (b) Felton, C. E.; Harding, L. P.; Jones, J. E.; Kariuki, B. M.; Pope, S. J. A.; Rice, C. R. *Chem. Commun.* **2008**, 6185–6187.
(23) (a) Jiang, P.; Chen, L.; Lin, J.; Liu, Q.; Ding, J.; Gao, X.; Guo, Z. *Chem. Commun.* **2002**, 1424–1425. (b) Mikata, Y.; Yamanaka, A.; Yamashita, A.; Yano, S. *Inorg. Chem.* **2008**, *47*, 7295–7301. (c) Nolan, E. M.; Jaworski, J.; Okamoto, K.; Hayashi, Y.; Sheng, M.; Lippard, S. J. *J. Am. Chem. Soc.* **2005**, *127*, 16812–16823. (d) Zhang, Y.; Guo, X.; Si, W.; Jia, L.; Qian, X. *Org. Lett.* **2008**, *10*, 473–476.
(24) (a) Dhara, K.; Karan, S.; Ratha, J.; Roy, P.; Chandra, G.; Manassero, M.; Mallik, B.; Banerjee, P. *Chem. Asian J.* **2007**, *2*, 1091–1100. (b) Gao, L.; Wang, Y.; Wang, J.; Huang, L.; Shi, L.; Fan, X.; Zou, Z.; Yu, T.; Zhu, M.; Li, Z. *Inorg. Chem.* **2006**, *45*, 6844–6850. (c) Li, N.; Xiang, Y.; Chen, X.; Tong, A. *Talanta* **2009**, *79*, 327–332.
(25) (a) Lu, C.; Xu, Z.; Cui, J.; Zhang, R.; Qian, X. *J. Org. Chem.* **2007**, *72*, 3554–3557. (b) Xue, L.; Liu, C.; Jiang, H. *Org. Lett.* **2009**, *11*, 1655–1658. (c) Xue, L.; Liu, Q.; Jiang, H. *Org. Lett.* **2009**, *11*, 3454–3457.
(26) Haugland, R. P. *Handbook of Fluorescent Probes and Research Chemicals*, 6th ed.; Spence, M. T. Z., Ed.; Molecular Probes: Eugene, OR, 1996; pp 530−540.
(27) (a) Kim, H. M.; Seo, M. S.; An, M. J.; Hong, J. H.; Tian, Y. S.; Choi, J. H.; Kwon, O.; Lee, K. J.; Cho, B. R. *Angew. Chem., Int. Ed.* **2008**, *47*, 5167–5170. (b) Jiang, W.; Fu, Q.; Fan, H.; Wang, W. *Chem. Commun.* **2008**, 259–261. (c) Komatsu, K.; Kikuchi, K.; Kojima, H.; Urano, Y.; Nagano, T. *J. Am. Chem. Soc.* **2005**, *127*, 10197–10204.
(28) Pope, S. J. A.; Layeb, R. H. *Dalton Trans.* **2006**, 3108–3113.
(29) (a) Xu, Z.; Kim, G.; Han, S.; Jou, M.; Lee, C.; Shin, I.; Yoon, J. *Tetrahedron* **2009**, *65*, 2307–2312. (b) Kawabata, E.; Kikuchi, K.; Urano, Y.; Kojima, H.; Odani, A.; Nagano, T. *J. Am. Chem. Soc.* **2005**, *127*, 818–819.

Scheme 1. (a) Amide Resonance and (b) Amide Tautomerization

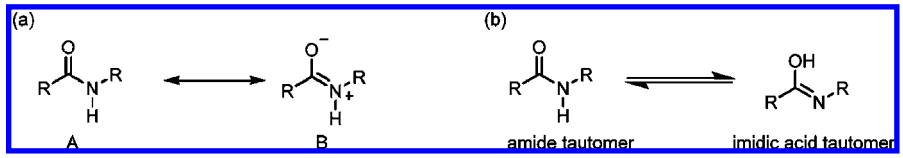

Scheme 2. Synthesis of **ZTRS** and **ZTF**

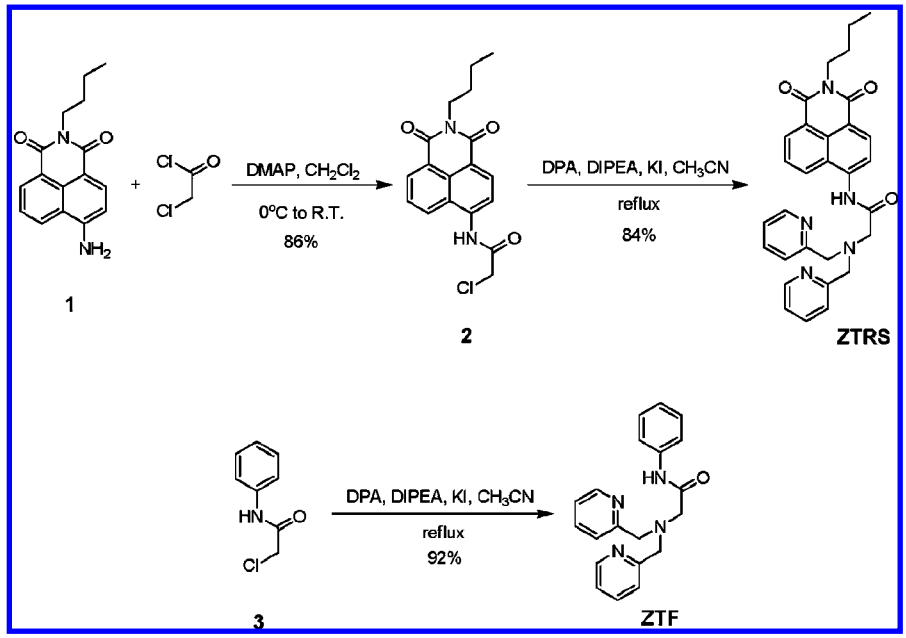

in sensors.[30] Dai et al. developed TPA-based sensors with a trigonal bipyramidal coordination geometry to improve the Zn^{2+}/Cu^{2+} selectivity.[30] In this contribution, an amide group is introduced into a DPA-type receptor to increase the Zn^{2+} selectivity. The amide linkage is a key facet in the structure of proteins, peptides, and other biologically important molecules.[31] The hindered C−N bond rotation of amides (the peptide bond) is due to amide resonance (Scheme 1a) and provides proteins with the ability to form secondary and tertiary structures fundamental to biological activity. In our scaffold, an amide group was inserted into a sensor (**ZTRS**) to link two moieties of the 1,8-naphthalimide fluorophore and a DPA chelator. 4-Aminonaphthalimide is a cell-permeable fluorophore possessing a visible emission wavelength, high photostability, and facile synthesis of various derivatives.[32] The amide oxygen and nitrogen atoms are well-known chelating sites.[33] The binding of Zn^{2+} to the amide-DPA receptor of **ZTRS** induced an enhanced shift in emission wavelength due to binary effects of photoinduced electron transfer (PET) and intermolecular charge transfer (ICT) mechanisms, and therefore displays a turn-on signal. More importantly, high binding selectivity for Zn^{2+} was achievable by complexation of various metal ions in alternative amide tautomeric forms (Scheme 1b).

Results and Discussion

Synthesis. The route used to synthesize **ZTRS** is initiated by the coupling of 4-amino-*N*-butyl-1,8-naphthalimide (**1**) and 2-chloroacetyl chloride to produce **2** in 86% yield (Scheme 2). Reaction of **2** with DPA under basic conditions gives **ZTRS** in 84% yield. As a reference compound, **ZTF** without a fluorophore was prepared by the condensation of 2-chloro-*N*-phenylacetamide with DPA in 92% yield.

Effect of pH on the Fluorescence of ZTRS. The influence of pH on the fluorescence of **ZTRS** was initially examined by fluorescence titration in acetonitrile/water (50:50) solution (Figure 1). The fluorescence spectrum of **ZTRS** exhibits an emission band with a maximum at 483 nm (ε = 83300 M^{-1} cm^{-1}, Φ = 0.016). Since the carbonyl group in **ZTRS** decreases the electron-donating ability of the amide nitrogen, ~40 nm blue-shift was observed in emission compared to that of 4-amino-1,8-naphthalimide (520−530 nm). The fluorescence of **ZTRS** at 483 nm remained unaffected between pH 12.8 and 6.3 but dramatically increased from pH 6.3 to 5.4 due to the inhibited PET process by protonation of the tertiary amine in DPA; with increasing acidity from pH 4.7 to 2.6, a significant decrease in the 483 nm emission and a blue-shifted emission band centered at 456 nm were observed. This phenomenon may be attributed to the protonation of the amide oxygen, which leads to a decrease in electron-donating ability and a blue-shift in emission. The stable fluorescence of **ZTRS** at around pH 7.0 is favorable for in vivo applications.

Zn^{2+} Selectivity. The selectivity of the fluorescent response of **ZTRS** to zinc ions was then examined. Figure 2a shows the

(30) Dai, Z.; Xu, X.; Canary, J. W. *Chem. Commun.* **2002**, *13*, 1414–1415.
(31) Greenberg, A.; Breneman, C. M.; Liebman, J. F. *The Amide Linkage: Structural Significance in Chemistry, Biochemistry, and Materials Science*; Wiley-Interscience: New York, 2000.
(32) Wang, J.; Xiao, Y.; Zhang, Z.; Qian, X.; Yang, Y.; Xu, Q. *J. Mater. Chem.* **2005**, *15*, 2836–2839.
(33) (a) Marlin, D. S.; Cabrera, D. G.; Leigh, D. A.; Slawin, A. M. Z. *Angew. Chem., Int. Ed.* **2006**, *45*, 77–83. (b) Patten, T. E.; Olmstead, M. M.; Troeltzsch, C. *Inorg. Chim. Acta* **2008**, *361*, 365–372. (c) Tsukube, H.; Noda, Y.; Kataoka, Y.; Miyake, H.; Shinoda, S.; Kojima-Yuasa, A.; Nishidab, Y.; Matsui-Yuasa, I. *Dalton Trans.* **2008**, *30*, 4038–4043.

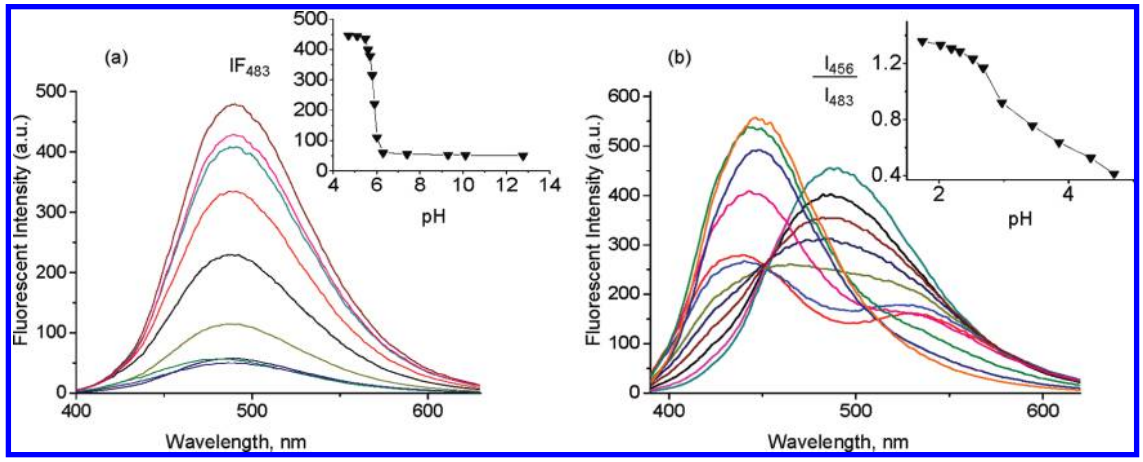

Figure 1. Influence of pH on the fluorescence of **ZTRS** in acetonitrile/water (50:50, v/v). Excitation wavelength: 360 nm. [**ZTRS**] = 10 μM. (a) pH 4.7−12.8. Inset: The fluorescence intensity at 483 nm as a function of pH; (b) pH 4.7−1.8. Inset: The ratiometric fluorescence changes as a function of pH.

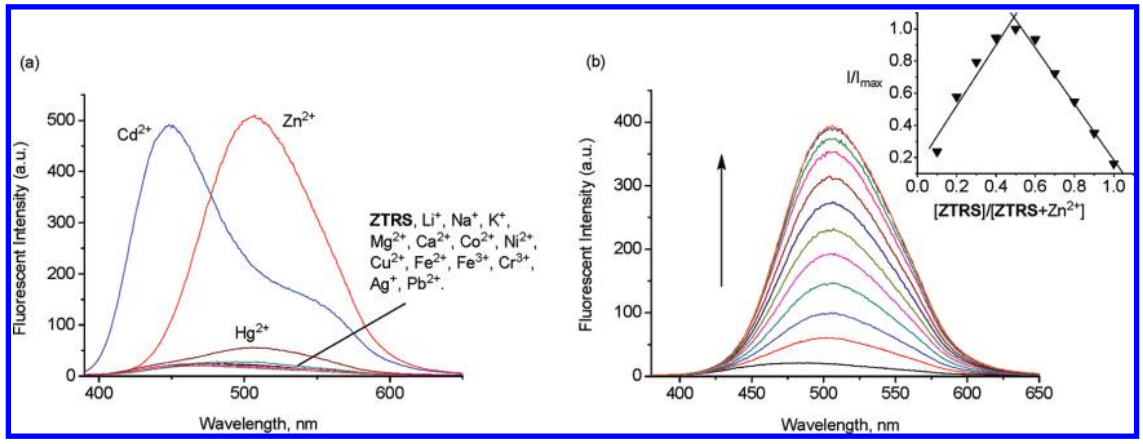

Figure 2. (a) Fluorescence spectra of 10 μM **ZTRS** in the presence of various metal ions in aqueous solution (CH_3CN/0.5 M HEPES (pH 7.4) = 50:50). Excitation at 360 nm. (b) Fluorescence spectra of **ZTRS** in the presence of different concentrations of Zn^{2+}. The inset shows the Job plot evaluated from the fluorescence with a total concentration of 10 μM.

fluorescence response of **ZTRS** to various metal ions in aqueous solutions (CH_3CN/0.5 M HEPES, pH 7.4 = 50:50). Selective and large fluorescent enhancements (FE) were observed upon addition of Cd^{2+} (21 fold) and Zn^{2+} (22 fold) to the solution of **ZTRS**. Notably, Cd^{2+} induced a blue-shift in the emission of **ZTRS** to 446 nm (blue fluorescence, $\varepsilon = 84700\ M^{-1}\ cm^{-1}$, $\Phi = 0.34$), while Zn^{2+} caused a red-shift to 514 nm (green fluorescence, $\varepsilon = 87500\ M^{-1}\ cm^{-1}$, $\Phi = 0.36$). This difference in response allows **ZTRS** to easily distinguish between Cd^{2+} and Zn^{2+} in aqueous solution, even with the naked eye (Figure 3). The Job plots indicate the **ZTRS**/Zn^{2+} and **ZTRS**/Cd^{2+} complexes all have 1:1 stoichiometry (Figure 2b and Supporting Information, Figure S1). The apparent dissociation constants (K_d) of **ZTRS** with Zn^{2+} and Cd^{2+} were determined by fluorescence spectroscopy as shown in Figure 4 to be 5.7 nM and 48.5 nM, respectively.[18b] In addition, **ZTRS** responds to metal ions in the same way in DMSO aqueous solutions (DMSO/0.5 M HEPES, pH 7.4 = 10:90) (Supporting Information, Figure S2). Also, it is worth mentioning that even in 100% aqueous solutions **ZTRS** can selectively sense Zn^{2+} (8 fold: $\varepsilon = 68600\ M^{-1}\ cm^{-1}$, $\Phi = 0.096$) and Cd^{2+} (7 fold: $\varepsilon = 63500\ M^{-1}\ cm^{-1}$, $\Phi = 0.084$) with less enhanced fluorescence (Supporting Information, Figure S3). The good water solubility of **ZTRS** demonstrates its potential for biological imaging.

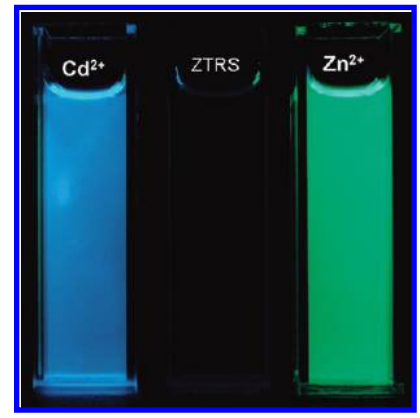

Figure 3. Visible emission observed from samples of **ZTRS**, **ZTRS**/Cd^{2+}, and **ZTRS**/Zn^{2+}.

In contrast to the fluorescent response of **ZTRS** to metal ions in aqueous solutions, in 100% CH_3CN Zn^{2+} and Cd^{2+} result in blue-shifted emissions with the maximum wavelength change from 481 to 430 and 432 nm, respectively (Supporting Information, Figures S4, S5); however, the addition of Zn^{2+} and Cd^{2+} to **ZTRS** in 100% DMSO cause red-shifted emissions with the maximum wavelength change from 472 to 512 and 532 nm, respectively (Supporting Information, Figures S6, S7). The

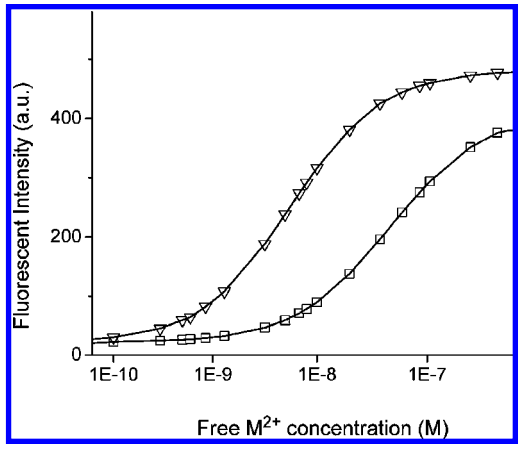

Figure 4. Fluorescence intensity of **ZTRS** (10 μM) as a function of free Zn^{2+} (∇, λ_{em} = 514 nm) or Cd^{2+} concentration ($\square$, λ_{em} = 446 nm).

Scheme 3. Different Binding Modes of **ZTRS** with Zn^{2+} or Cd^{2+} in CH_3CN, DMSO, and Aqueous Solution

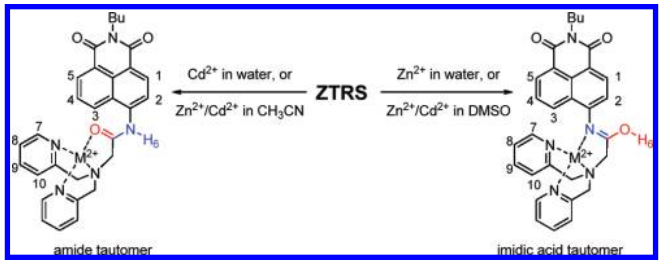

addition of other HTM ions results in blue-shift in emissions in both CH_3CN and DMSO (Supporting Information, Figures S8, S9). However, a small blue-shift of the absorption maximum of **ZTRS** in CH_3CN, DMSO, and aqueous solution upon addition of Zn^{2+} and Cd^{2+} (Supporting Information, Figures S10−S15) indicates that the red-shifted emission does not result from the deprotonation of amide NH group, because the deprotonation of the NH group conjugated to 1,8-naphthalimide would cause a red-shift in absorption spectra. [18h,25a] These spectral data suggest that **ZTRS** binds Zn^{2+} and Cd^{2+} in different tautomeric forms, depending on the solvent and metal ions (Scheme 3); **ZTRS** complexes both Zn^{2+} and Cd^{2+} in the amide tautomer in CH_3CN, and the imidic acid tautomer in DMSO predominantly. However, other HTM ions bind to the amide tautomer in both CH_3CN and DMSO.

Further evidence for the amide and imidic acid tautomeric binding modes (Scheme 3) is provided by ^{1}H NMR titration experiments of **ZTRS** with Zn^{2+} and Cd^{2+} in CD_3CN (Supporting Information, Figures S16, S17) and DMSO-d_6 (Supporting Information, Figures S18, S19), 2D NOESY of **ZTRS**/Zn^{2+} (1:1 complex) in CD_3CN (Figures 3, Supporting Information, Figures S20, S21) and DMSO-d_6 (Figures 3, S22−23), and IR spectra of **ZTRS**/Zn^{2+} (1:1 complex) in CH_3CN (Supporting Information, Figure S24) and DMSO (Supporting Information, Figure S25). As a reference, the binding properties of **ZTF** with Zn^{2+} were also examined by means of ^{1}H NMR and IR spectra.

The blue-shifts in emission of **ZTRS** with HTM ions in acetonitrile are attributed to the coordination of the amide oxygen with metal ions which increases the electron-withdrawing ability of the amide group via ICT mechanism. As expected, the absorption maximum of **ZTRS** undergoes a blue-shift from 371 to 348 nm upon addition of both Zn^{2+} and Cd^{2+} (Supporting Information, Figures S10, S11). ^{1}H NMR analysis provides further evidence to support the M−O bond formation, which results in large upfield shifts of the resonance of the adjacent NH proton.[34] For example, addition of 1 equiv of Zn^{2+} or Cd^{2+} promotes a large upfield shift (11.72 to 9.73 and 9.49 ppm, respectively) of the resonance of the adjacent NH proton in **ZTRS** (Supporting Information, Figures S16, S17). In contrast, the same proton in **ZTRS** in CD_3CN with the addition of 1 equiv of Zn^{2+} and Cd^{2+} (Supporting Information, Figures S18, S19), undergoes a much smaller upfield shift from 11.51 to 11.26 and 11.37 ppm in DMSO, respectively. ^{1}H NMR analysis of **ZTF** with Zn^{2+} also shows a large upfield shift of NH from 10.91 to 9.29 in CD_3CN, while there is a clear downfield shift of OH from 10.54 to 10.75 in DMSO (Figure 5). With the electron-withdrawing nature of the carbonyl group, the lone pair of electrons on the amide nitrogen is delocalized by resonance, thus forming a partial double bond with the carbonyl carbon and putting a partial negative charge on the oxygen (amide resonance, Scheme 1a). The complexation of the carbonyl oxygen with Zn^{2+} in CD_3CN blocks the resonance structure B and then shifts the NH resonance upfield. Correspondingly, the binding of the amide nitrogen with Zn^{2+} in DMSO acts as an electron-withdrawing group to shift the OH resonance downfield. Therefore, the chemical shift of the amide NH can be used to distinguish between whether Zn^{2+} (or other metal ions) is bound to carbonyl oxygen or imidic acid nitrogen.

The single crystal structure and data of **ZTF**-Zn^{2+} in CH_3CN are shown in Figure 6 and Supporting Information, Table S1, respectively. As expected, the amide oxygen (O1) cooperates with the DPA (N2−N4) and one CH_3CN molecule (N5) as a receptor to bind Zn^{2+} (Figure 6). The bond length of Zn(1)−O(1) (2.002 Å) is much shorter than the other four Zn1−N bonds.

2D NOESY studies of **ZTRS**/Zn^{2+} (1:1) in CD_3CN and DMSO-d_6 give the direct evidence for the amide and imidic acid tautomeric binding modes (Figure 7). In NOESY, the nuclear Overhauser effect (NOE) between nuclear spins is used to establish the correlations. Hence the cross-peaks in the resulting two-dimensional spectrum connect resonances from spins that are spatially close. As shown in Figure 7, in the amide tautomeric form, H4 and H6 are spatially far, so there are only cross peaks between H2−H6 and H3−H6, but in the imidic acid tautomeric form, H4 and H6 are spatially close, so that besides those between H2−H6 and H3−H6, there is also a strong cross peak between H4−H6 which supports the existence of the OH proton.

IR spectra also confirm the imidic acid binding mode. As shown in Supporting Information, Figure S24, the IR spectrum of **ZTRS**/Zn^{2+} (1:1) complex in CH_3CN displays a typical C=O amide *I* band (1662 cm^{-1}) and C−N stretching absorption at 1099 cm^{-1}. The typical O−H (3457 cm^{-1}) and C−O (1102 cm^{-1}) stretching absorptions further verify the **ZTRS**/Zn^{2+} (1:1) complex in DMSO has the imidic acid binding pattern (Supporting Information, Figure S25). The IR spectrum of **ZTF**/Zn^{2+} (1:1) complex in DMSO also exhibits an O−H stretching absorption (Supporting Information, Figure S27).

Significantly therefore, we conclude that in aqueous solutions of Cd^{2+} the receptor **ZTRS** adopts an amide tautomer binding mode showing blue-shifted emission, while in aqueous solutions of Zn^{2+} **ZTRS** binds the metal ion via an imidic acid tautomer,

(34) A paper that reported the binding of amide oxygen with HTM ions resulting in upfield shifts of the resonance of the adjacent NH proton in ^{1}H NMR spectra; ref 33a.

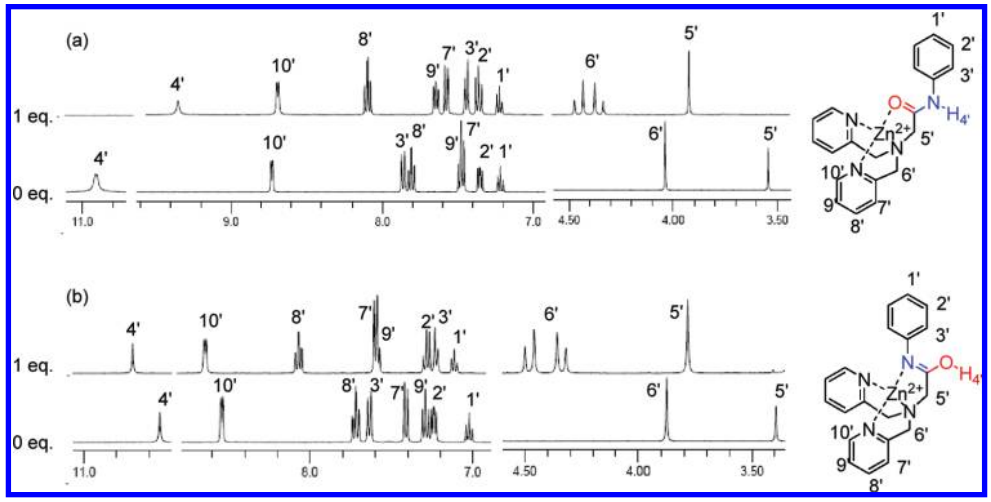

Figure 5. ^{1}H NMR spectra of **ZTF** in the presence of Zn^{2+} in (a) CD_3CN and (b) DMSO-d_6.

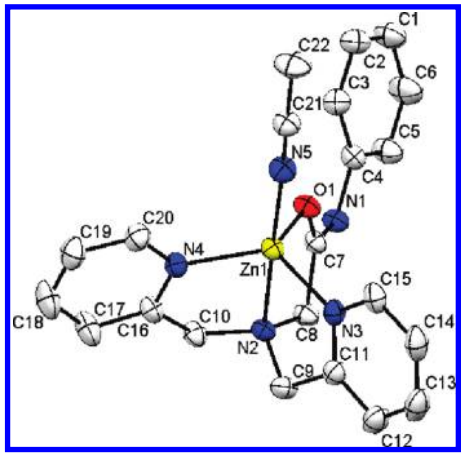

Figure 6. Crystal structure of **ZTF**-Zn^{2+}. All hydrogen atoms and perchlorate counterions are omitted for clarity. Thermal ellipsoids are shown at the 50% probability level. Selected bond distances (Å) and bond angles (deg): Zn(1)−O(1) = 2.002(1), Zn(1)−N(2) = 2.206(1), Zn(1)−N(3) = 2.046(1), Zn(1)−N(4) = 2.033(2), Zn(1)−N(5) = 2.045(2), O(1)−Zn(1)−N(2) = 80.65(5), O(1)−Zn(1)−N(3) = 114.68(5), O(1)−Zn(1)−N(4) = 119.02(6), O(1)−Zn(1)−N(5) = 95.44(6), N(2)−Zn(1)−N(3) = 80.65(5), N(2)−Zn(1)−N(4) = 80.72(5), N(2)−Zn(1)−N(5) = 176.04(6), N(3)−Zn(1)−N(4) = 118.54(6), N(3)−Zn(1)−N(5) = 101.29(6), N(4)−Zn(1)−N(5) = 101.20(6).

showing red-shifted emission. The red-shift in emission of **ZTRS**/Zn^{2+} is likely to be due to the expansion of the fluorophore-conjugated system.

To further check the Zn^{2+}-selective tautomeric transformation of **ZTRS** over other metal ions, competition experiments were conducted in the presence of 300 equiv of Na^+, K^+, Mg^{2+}, or Ca^{2+} and 3 equiv of Li^+, Co^{2+}, Ni^{2+}, Cu^{2+}, Cd^{2+}, Fe^{2+}, Fe^{3+}, Cr^{3+}, Ag^+, Hg^{2+}, or Pb^{2+}, with the subsequent addition of 1 equiv of Zn^{2+}. As shown in Figure 8a, the emission profile of the **ZTRS**/Zn^{2+} complex is unperturbed in the presence of these metal ions, indicating the strongest affinity and selectivity for Zn^{2+}. A reasonable explanation would be the displacement of these metal ions by Zn^{2+} and the induced transformation of chelation from an amide to an imidic acid tautomeric form. It is notable that the addition of Zn^{2+} to these solutions induced an immediate **ZTRS**/Zn^{2+} fluorescence profile except in Cu^{2+} solution. The Cu^{2+} solution with 1 equiv Zn^{2+} displayed an enhanced fluorescence centered at 514 nm after 48 h.

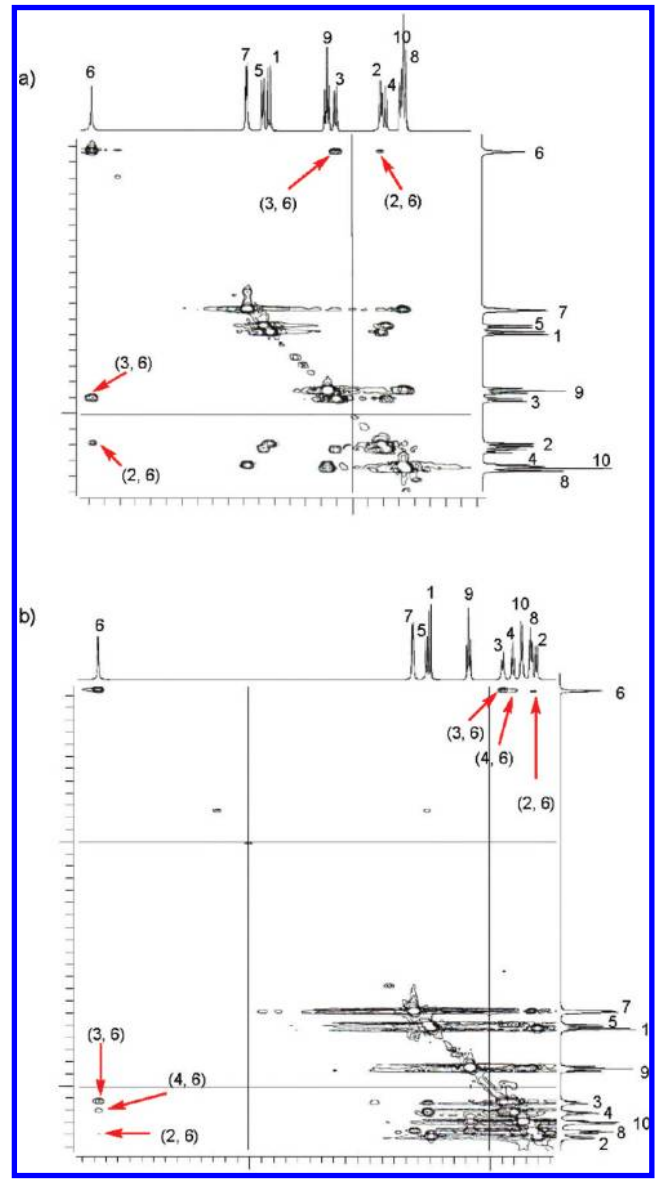

Figure 7. Partial 500 MHz ^{1}H−^{1}H NOESY spectra of **ZTRS**/Zn^{2+} (1:1) in (a) CD_3CN and (b) DMSO-d_6.

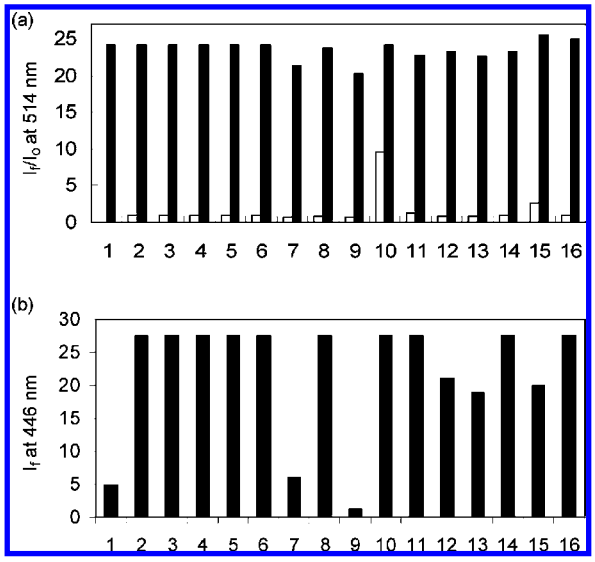

Figure 8. (a) Fluorescence responses of 10 μM **ZTRS** to various metal ions in aqueous solution (CH_3CN/0.5 M HEPES (pH 7.4) = 50:50). Excitation at 360 nm. Bars represent the final fluorescence intensity at 514 nm (I_f) over the original emission at 514 nm (I_o). White bars represent the addition of 3 equiv of metal ions (for Na^+, K^+, Mg^{2+}, and Ca^{2+}, 300 equiv) to a 10 μM solution of **ZTRS**. Black bars represent the subsequent addition of 1 equiv of Zn^{2+} to the solution. (b) Fluorescence responses of 10 μM **ZTRS**/Cd^{2+} complex (1:1) to various metal ions (30 μM, for Na^+, K^+, Mg^{2+}, and Ca^{2+}, 3 mM) in aqueous solution (CH_3CN/0.5 M HEPES (pH 7.4) = 50:50). Excitation at 360 nm. (1) Zn^{2+}, (2) Li^+, (3) Na^+, (4) K^+, (5) Mg^{2+}, (6) Ca^{2+}, (7) Co^{2+}, (8) Ni^{2+}, (9) Cu^{2+}, (10) Cd^{2+}, (11) Fe^{2+}, (12) Fe^{3+}, (13) Cr^{3+}, (14) Ag^+, (15) Hg^{2+}, (16) Pb^{2+}. Binding competition measurements were acquired after equilibration for 5 min.

The selectivity of the fluorescence responses of **ZTRS** to Cd^{2+} was also examined by the addition of various metal ions to the solution of **ZTRS**−Cd^{2+} complex (1:1). As shown in Figure 8b, the addition of Zn^{2+}, Co^{2+}, or Cu^{2+} quenches the fluorescence of **ZTRS**−Cd^{2+} complex at 446 nm. In contrast, other metal ions promote slight changes in the fluorescence of **ZTRS**−Cd^{2+} complex. This may mean that **ZTRS** has a higher affinity with Cd^{2+} than most of the HTM ions except for Zn^{2+}, Co^{2+}, and Cu^{2+}.

Ratiometric Detection of Zn^{2+} Based on the Displacement Approach. The addition of Zn^{2+} to **ZTRS** induces an enhanced fluorescence with a 31 nm red-shift in emission. For practical applications, ratiometric signal should show a large shift in absorption or emission. Most of the reported ratiometric Zn^{2+} sensors are constructed on the basis of an ICT mechanism.[18] Here, we develop a new approach to detect Zn^{2+} ratiometrically relying on a displacement strategy. In the displacement assay approach pioneered by Anslyn,[35] an indicator is first allowed to bind reversibly to a receptor. Then, a competitive analyte is introduced into the system causing the displacement of the indicator from the host, which in turn modulates an optical signal. Based on this principle, the major requirement for an indicator displacement approach is that the affinity between the indicator and the receptor should be comparable to that between the analyte and the receptor. In our case, the affinity of **ZTRS** with Zn^{2+} (K_d = 5.7 nM) is stronger than that with Cd^{2+} (K_d = 48.5 nM). The **ZTRS**/Cd^{2+} complex displays a broadband with a maximum at 446 nm. When Zn^{2+} was added to the solution of **ZTRS**/Cd^{2+} complex, Cd^{2+} was displaced by Zn^{2+}, resulting

(35) Nguyena, B. T.; Anslyn, E. V. *Coord. Chem. Rev.* **2006**, *250*, 3118–3127.

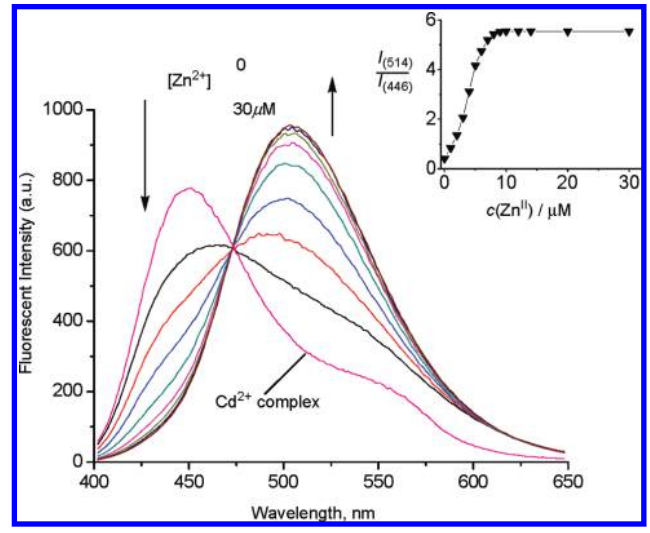

Figure 9. Fluorescence spectra of 10 μM **ZTRS**/Cd^{2+} in the presence of different concentrations of Zn^{2+} in aqueous solution (CH_3CN/0.5 M HEPES (pH 7.4) = 50:50). Excitation at 360 nm. Inset: Ratiometric calibration curve I_{514}/I_{446} as a function of Zn^{2+} concentration.

in a significant decrease in the 446 nm emission and an increase of a red-shifted emission band centered at 514 nm (attributed to the formation of a **ZTRS**/Zn^{2+} complex) with a clear isoemission point at 472 nm (Figure 9). The inset in Figure 9 exhibits the dependence of the intensity ratios of emission at 514 nm to that at 446 nm (I_{514}/I_{446}) on Zn^{2+}.

Detection of Intracellular Zn^{2+} with ZTRS. In vitro studies demonstrated the ability of **ZTRS** to detect Zn^{2+} with excellent selectivity. To examine whether this ability is preserved in vivo, A549 cells (lung cancer cells) were used to detect exogenous zinc ions in live cells. The cells treated with 5 μM **ZTRS** alone exhibited very weak background fluorescence (Figure 10a). However, the cells incubated with 1 μM $ZnCl_2$ and **ZTRS** displayed enhanced green fluorescence (Figure 10b). When the cells exposed to **ZTRS** and Zn^{2+} were further treated with a membrane-permeable zinc chelator (*N,N,N′,N′*-tetrakis(2-pyridylmethyl)ethylenediamine, TPEN) that decreases the intracellular level of zinc,[14b] the treated cells showed a very weak fluorescent signal, indicating that green fluorescence is caused by response of **ZTRS** to intracellular zinc ions (Figure 10c). Interestingly, while blue fluorescence was observed in cells incubated with 5 μM $CdCl_2$ and **ZTRS**, the cells initially treated with $CdCl_2$ and **ZTRS** and subsequent exposure of the cells to 1 μM $ZnCl_2$ exhibited green fluorescence (Figure 10d,e). These experiments indicate **ZTRS** can discriminate in vivo Zn^{2+} and Cd^{2+} with green and blue fluorescence, respectively. More attractively, Zn^{2+} could be ratiometrically detected in vivo with a large fluorescence color change from blue to green via the Cd^{2+} displacement approach. Furthermore, intracellular zinc ions were detected by use of **ZTRS** even in the presence of iron ions (Figure 10f,g). The cadmium-displacement method provides an appealing ratiometric change but this assay may have a drawback due to the toxicity of cadmium in biological systems. However, cytotoxicity of cadmium ions was not observed up to 40−50 μM concentrations, and thus this assay could be applied for biological systems. These cell experiments show that **ZTRS** is cell-permeable and can be used to monitor Zn^{2+} selectively in vivo and to further distinguish between Cd^{2+} and Zn^{2+} in living cells.

Imaging of Intact Zn^{2+} in Zebrafish with ZTRS. We then applied **ZTRS** to trace the distribution of intact zinc ions in

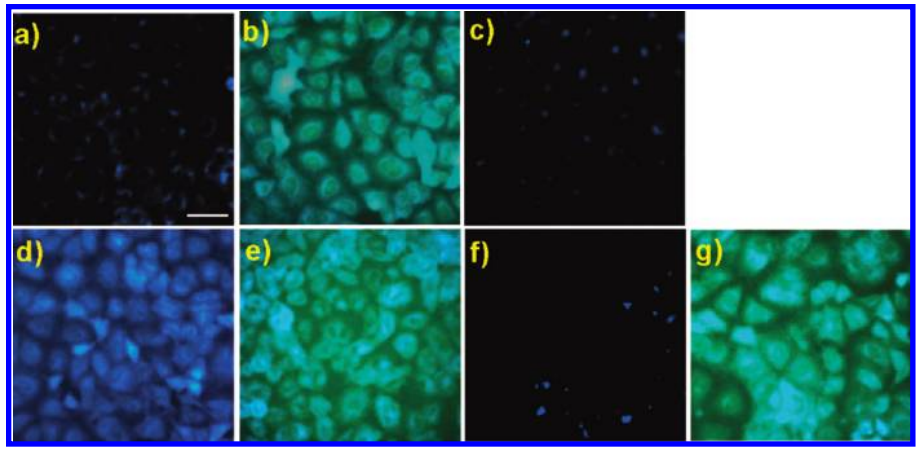

Figure 10. Fluorescence images of A549 cells incubated with 5 μM **ZTRS** and ions. Cells treated with **ZTRS** (a) in the absence and (b) presence of 1 μM of external zinc ions, and (c) after treatment with **ZTRS** and 1 μM $ZnCl_2$ and subsequent treatment of the cells with 25 μM TPEN. (d) Cells treated with **ZTRS** and 5 μM $CdCl_2$ and (e) after treatment with **ZTRS** and 5 μM $CdCl_2$ and subsequent treatment of the cells with 1 μM $ZnCl_2$. (f) Cells treated with **ZTRS** and 5 μM $Fe(ClO_4)_2$ and (g) after treatment with **ZTRS** and 5 μM $Fe(ClO_4)_2$ and subsequent treatment of the cells with 1 μM $ZnCl_2$ (bar = 50 μm).

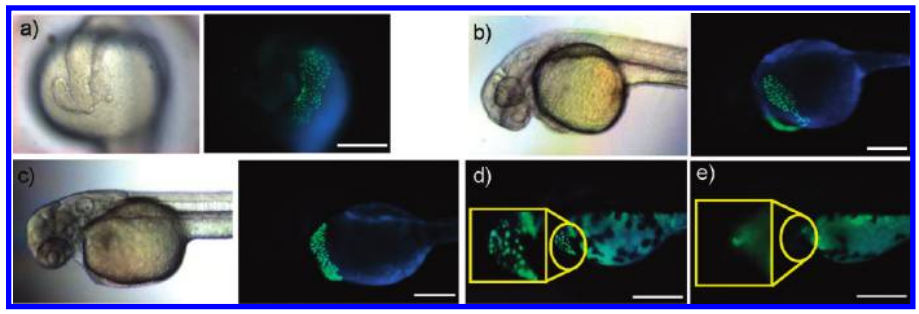

Figure 11. Zebrafish incubated with 5 μM **ZTRS**. (a) Images of 19 h-old, (b) 36 h-old, and (c) 48 h-old zebrafish incubated with **ZTRS** for 1 h. (d) Image of 54 h-old zebrafish incubated with **ZTRS** for 1 h, (e) image of 54 h-old zebrafish after initial incubation with 100 μM TPEN for 1 h, and subsequent treatment of washed zebrafish with **ZTRS** for 1 h (a, b, c: left, bright field images; right, fluorescence images). Scale bar = 250 μm.

living organisms. Zebrafish is a good animal model to monitor ions using sensors due to convenient detection of ions by fluorescence microscopy and permeability of ions and sensors in fish. Therefore, zebrafish recently has been widely used to detect various ions such as Hg^{2+}, Cu^{2+}, and Zn^{2+}.[17,36] Zebrafish embryos were incubated with 5 μM **ZTRS** at various time points during development.[36] At 19 h post fertilization (hpf) of the embryo, a green-spotted band was observed in the bottom of the venter (Figure 11a).[17] During development, the necklace-like band composed of green spots was brighter and moved to the top of the venter until 48 hpf (Figure 11b,c). After 54 hpf, the green-spotted band was no longer observed, and only scattered bright spots were distributed around the pericardial sac (Figure 11d). The treatment of 54 h-old zebrafish with 100 μM TPEN resulted in the disappearance of the green spots (Figure 11e). The green-spotted band may result from sequestration of **ZTRS** or an endogeneous zinc pool in fish. It was observed that, when 54 h-old zebrafish were exposed to external Zn^{2+} (20 μM) followed by treatment with **ZTRS**, overall green fluorescence in the fish was increased. This suggests that the green-spotted band may result from endogeneous zinc ions in fish and not sequestration of the probe. In a recent study, Guo and co-workers found quite similar green spots in the zebrafish stained with a NBD-based sensor (**NBD−TPEA**).[17] With the preliminary in vivo Zn^{2+} imaging of intact 4-day-old zebrafish larvae with **NBD−TPEA** staining, TPEN addition experiment of 5-day-old larvae, and the evidence of ICP-MS data for zinc in the separated zygomorphic luminescent areas, Guo and co-workers believe the green spots in zebrafish with **NBD−TPEA** staining are correlated to Zn^{2+} storage for the development of zebrafish. No abnormal developmental defects were observed upon treatment with **ZTRS**, indicating that it is biologically orthogonal. These results demonstrated the usefulness of **ZTRS** for monitoring biologically relevant ions in living organisms.

Conclusion

We have designed and synthesized a new naphthalimide-based fluorescent probe **ZTRS** for ratiometric Zn^{2+} sensing which contains an amide-DPA receptor. **ZTRS** has the strongest affinity with Zn^{2+} among competitive metal ions and displays an excellent fluorescent selectivity for Zn^{2+} with an enhanced red-shift in emission resulting from the Zn^{2+}-triggered amide tautomerization. Although **ZTRS** can bind to both Zn^{2+} and Cd^{2+}, these metal ions can be differentiated by this sensor; upon binding to Zn^{2+} and Cd^{2+} to the sensor, green and blue fluorescence were observed, respectively. Also, ratiometric detection of Zn^{2+} with a large emission wavelength shift from 446 to 514 nm can be achieved via a Cd^{2+} displacement

(36) (a) Ko, S.-K.; Yang, Y.-K.; Tae, J.; Shin, I. *J. Am. Chem. Soc.* **2006**, *128*, 14150–14155. (b) Yang, Y.-K.; Ko, S.-K.; Shin, I.; Tae, J. *Nat. Protocols* **2007**, *2*, 1740–1745. (c) Santra, M.; Ryu, D.; Chatterjee, A.; Ko, S.-K.; Shin, I.; Ahn, K. H. *Chem. Commun.* **2009**, 2115–2117. (d) Swamy, M. K.; Ko, S.-K.; Kwon, S. K.; Lee, H. N.; Mao, C.; Kim, J.-M.; Lee, K.-H.; Kim, J.; Shin, I.; Yoon, J. *Chem. Commun.* **2008**, 5915–5917.

approach. Furthermore, this sensor is cell permeable and can be applied to trace zinc ions during the development of a living organism. The connection of the amide-DPA with other fluorophores is in progress.

Experimental Section

Materials and Methods. Unless otherwise noted, materials were obtained from Aldrich and were used without further purification. The synthesis of compound **1** was according to the published procedure.[37] Melting points were measured using a Büchi 530 melting point apparatus. ^{1}H NMR and ^{13}C NMR spectra were recorded using Bruker 250 MHz or Varian 500 MHz. Chemical shifts were given in ppm and coupling constants (*J*) in Hz. UV absorption spectra were obtained on UVIKON 933 double beam UV/vis spectrometer. Fluorescence emission spectra were obtained using RF-5301/PC spectrofluorophotometer (Shimadzu).

Synthesis of Compound 2. A solution of 102 mg (0.9 mmol) of 2-chloroacetyl chloride in 5 mL of dry CH_2Cl_2 was added dropwise to a solution of 200 mg (0.75 mmol) 4-amino-*N*-butyl-1,8-naphthalimide (**1**) and 150 mg (1.23 mmol) 4-dimethylaminopyridine (DMAP) in 30 mL of dry CH_2Cl_2 stirred in an ice bath. After stirred 2 h at room temperature, the mixture was removed under reduced pressure to obtain a pale-yellow solid, which was purified by silica gel column chromatography using dichloromethane as eluent to afford 4-(2-chloroacetyl)amino-*N*-butyl-1,8-naphthalimide (**2**). Yield: 221 mg (86%). Mp: 243−244 °C. ^{1}H NMR ($CDCl_3$, 250 MHz) δ 0.98 (t, J = 7.2 Hz, 3H), 1.39−1.48 (m, J = 7.2 Hz, 2H), 1.57−1.74 (m, J = 7.2 Hz, 2H), 4.16 (t, J = 7.2 Hz, 2H), 4.39 (s, 2H), 7.80 (t, J = 8.4 Hz, 1H), 8.16 (d, J = 8.5 Hz, 1H), 8.45 (d, J = 8.0 Hz, 1H), 8.61 (m, 2H), 9.15 (s, 1H, N−H). ^{13}C NMR ($CDCl_3$, 62.5 MHz) δ 13.86, 20.38, 30.18, 40.31, 43.39, 119.02, 119.65, 123.54, 123.80, 125.66, 127.23, 128.80, 131.34, 132.08, 137.0, 163.45, 163.95, 164.19. HRMS (ESI) calcd for $C_{18}H_{18}ClN_2O_3$ [MH^+] 345.1017, found 345.1006.

Synthesis of ZTRS. 4-(2-Chloroacetyl)amino-*N*-butyl-1,8-naphthalimide (**2**) (100 mg, 0.29 mmol), di-(2-picolyl)amine (DPA) (70 mg, 0.35 mmol), *N,N*-diisopropylethylamine (DIPEA) (0.5 mL), and potassium iodide (30 mg) were added to acetonitrile (50 mL). After stirring and refluxing for 10 h under nitrogen atmosphere, the mixture was cooled to room temperature, and the mixture was removed under reduced pressure to obtain a yellow oil, which was purified by silica gel column chromatography (CH_2Cl_2:MeOH = 100:1) to afford 4-(2-(di-(2-picolyl)amino)acetyl)amino-*N*-butyl-1,8-naphthalimide (**ZTRS**). Yield: 124 mg (84%). Mp: 138−139 °C. ^{1}H NMR ($CDCl_3$, 250 MHz) δ 0.87 (t, J = 7.2 Hz, 3H), 1.33−1.39 (m, J = 7.2 Hz, 2H), 1.60−1.65 (m, J = 7.2 Hz, 2H), 3.55 (s, 2H), 3.98 (s, 4H), 4.07 (t, J = 7.2 Hz, 2H), 7.06 (t, J = 6.2 Hz, 2H), 7.24 (m, 2H), 7.52 (t, J = 7.6 Hz, 2H), 7.74 (t, J = 7.8 Hz, 1H), 8.35−8.46 (m, 3H), 8.54 (t, J = 8.4 Hz, 2H), 8.98 (d, J = 8.4 Hz, 1H), 11.64 (s, 1H). ^{13}C NMR ($CDCl_3$, 62.5 MHz) δ 13.87, 20.38, 30.19, 40.10, 59.11, 60.57, 116.95, 117.56, 122.69, 122.96, 123.38, 126.20, 128.18, 128.97, 131.01, 132.61, 136.71, 139.78, 149.54, 157.62, 163.70, 164.31, 170.79. HRMS (ESI) calcd for $C_{30}H_{30}N_5O_3$ [MH^+] 508.2349, found 508.2344.

Synthesis of ZTF. Using the same procedure as that for **ZTRS**, combining 2-chloro-*N*-phenylacetamide (**3**) (200 mg, 1.18 mmol) and di-(2-picolyl)amine (DPA) (235 mg, 1.18 mmol) produced 360 mg of **ZTF** (92% yield) as a pale-brown oil. ^{1}H NMR ($CDCl_3$, 400 MHz) δ 3.44 (s, 2H), 3.87 (s, 4H), 7.03 (t, J = 7.4 Hz, 1H), 7.09 (t, J = 6.2 Hz, 2H), 7.21 (d, J = 7.6 Hz, 2H), 7.29 (t, J = 8.0 Hz, 2H), 7.53 (t, J = 7.6 Hz, 2H), 7.77 (d, J = 7.2 Hz, 2H), 8.55 (d, J = 4.8 Hz, 2H), 10.90 (s, 1H, amide). ^{13}C NMR ($CDCl_3$, 62.5 MHz) δ 59.18, 60.65, 120.00, 122.89, 123.59, 124.10, 129.22, 137.00, 139.14, 149.75, 158.50, 170.16. HRMS (ESI) calcd for $C_{20}H_{21}N_4O$ [MH^+] 339.1739, found 339.1729.

Synthesis of ZTF−Zn(ClO$_4$)$_2$. A solution of $Zn(ClO_4)_2 \cdot 6H_2O$ (123 mg, 0.33 mmol) in 1 mL of dry CH_3CN was dropwise added to the solution of **ZTF** (100 mg, 0.3 mmol) in 2 mL of dry CH_3CN. The solution was stirred for another half hour. Colorless crystals of **ZTF−Zn(ClO$_4$)$_2$** were obtained by vapor diffusion of ether into the above CH_3CN solution.

Determination of Quantum Yield. The quantum yields of fluorescence were determined by comparison of the integrated area of the corrected emission spectrum of the samples with a reference of *N*-butyl-4-butylamino-1,8-naphthalimide in absolute ethanol (Φ = 0.810).[38] For the metal-free study, 5 mL of 10 μM **ZTRS** in aqueous solution (CH_3CN/0.5 M HEPES (pH 7.4) = 50:50) was prepared. For the metal-bound studies, 15 μL of 10 mM $Zn(ClO_4)_2$ or $Cd(ClO_4)_2$ was added to 5 mL of 10 μM **ZTRS** in aqueous solution (CH_3CN/0.5 M HEPES (pH 7.4) = 50:50). The concentration of the reference was adjusted to match the absorbance of the test sample at the wavelength of excitation. Emission for **ZTRS** was integrated from 375 to 650 nm with excitation at 360 nm. The quantum yields were calculated with the expression in eq 1.

$$\Phi_{\text{sample}} = \Phi_{\text{standard}} \times \frac{\int \text{emission}_{\text{sample}}}{\int \text{emission}_{\text{standard}}} \qquad (1)$$

X-ray Crystallographic Analysis. Single crystals were cooled to 180 K immediately after removal from the solution, and single crystal X-ray diffraction data were collected at 180 K on a Nonius Kappa CCD diffractometer using MoKa radiation (λ = 0.71073 Å) equipped with an Oxford Cryosystem cryostream. The structure was solved by direct methods using the program SHELXS-97 and refined on F^2 against all data using SHELXL-97. All non-hydrogen atoms were refined with anisotropic displacement parameters. The hydrogen atoms were included in the models in calculated positions and were refined as constrained to bonding atoms.

Determination of Apparent Dissociation Constant. Fluorescence spectroscopy was used to determine the apparent dissociation constants (K_d) of **ZTRS** (10 μM) with Zn^{2+} and Cd^{2+}, using the reported method.[18b] Free Zn^{2+} and Cd^{2+} concentrations were controlled by metal ion buffers (e.g., NTA (nitrilotriacetic acid) in this study, 10 mM). log K (ZnNTA) = 10.66 (20 °C, = 0.1), and log K (CdNTA) = 9.80 (20 °C, = 0.1).[39] The fluorescence intensity data (Figure 4) were fitted to eq 2, and K_d was calculated,

$$F = F_0 + (F_{\max} - F_0)\frac{[M^{2+}]_{\text{free}}}{K_d + [M^{2+}]_{\text{free}}} \qquad (2)$$

where F is the fluorescence intensity, $F_{\max}$ is the maximum fluorescence intensity, F_0 is the fluorescence intensity with no addition of Zn^{2+} and Cd^{2+}, and $[M^{2+}]_{\text{free}}$ is the free Zn^{2+} and Cd^{2+} concentration.

Imaging of Mammalian Cells Incubated with ZTRS and CdCl$_2$ or ZnCl$_2$. A549 cells (human lung cancer cells) were seeded in a 24-well plate at a density of 2×10^3 cells per well in culture media (RPMI-1640 supplemented with 10% fetal bovine serum (FBS)). After 24 h, 5 μM **ZTRS** in the culture media containing 0.1% (v/v) DMSO was added to the cells, and the cells were incubated for 1 h at 37 °C. After washing twice with 400 μL of Dulbecco's phosphate buffered saline (DPBS, without calcium and magnesium) to remove the remaining sensor, the cells were further treated with 5 μM $CdCl_2$ or 1 μM $ZnCl_2$ in DPBS for 15 min. The treated cells were imaged by fluorescence microscopy (Eclipse TE2000-S, Nikon, Japan).

For a cadmium-displacement experiment, 5 μM **ZTRS** in the culture media containing 0.1% (v/v) DMSO was added to the cells, and the cells were incubated for 1 h at 37 °C. After washing twice with 400 μL of DPBS to remove the remaining sensor, the cells

(37) Liu, B.; Tian, H. *Chem. Commun.* **2005**, 3156–3158.

(38) Alexiou, M. S.; Tychopoulos, V.; Ghorbanian, S.; Tyman, J. H. P.; Brown, R. G.; Brittain, P. I. *J. Chem. Soc. PERKIN TRANS.* **1990**, *2*, 837–842.

(39) Anderegg, G. *Pure Appl. Chem.* **1982**, *54* (12), 2693–2758.

were treated with 5 μM $CdCl_2$ in DPBS for 15 min. Without washing, the cells were further treated with 1 μM $ZnCl_2$ for 15 min. The treated cells were imaged by fluorescence microscopy.

For a TPEN experiment, 5 μM **ZTRS** in the culture media containing 0.1% (v/v) DMSO was added to the cells, and the cells were incubated for 1 h at 37 °C. After washing twice with 400 μL of DPBS to remove the remaining sensor, the cells were treated with 1 μM $ZnCl_2$ in DPBS for 15 min. Without washing, the cells were further treated with 25 μM TPEN for 15 min. The treated cells were imaged by fluorescence microscopy.

For an iron competition experiment, 5 μM **ZTRS** in the culture media containing 0.1% (v/v) DMSO was added to the cells, and the cells were incubated for 1 h at 37 °C. After washing twice with 400 μL of DPBS to remove the remaining sensor, the cells were treated with 5 μM $Fe(ClO_4)_2$ in DPBS for 15 min. Without washing, the cells were further treated with 1 μM $ZnCl_2$ for 15 min. The treated cells were imaged by fluorescence microscopy.

Fluorescence images were obtained as the following: the excitation wavelength range of the UV-2A filter is from 330 to 380 nm, including 360 nm of the maximum excitation wavelength of the **ZTRS**. The long-pass emission (barrier) filter employed in the UV-2A combination is designed to collect signals at wavelengths exceeding 420 nm, enabling visualization of red, green, and blue emission from fluorophores excited in the ultraviolet. Under this UV-2A filter, the cells treated with $CdCl_2$ and $ZnCl_2$ show blue and greenish-blue, respectively.

Tracing Distribution of Zinc Ions in Zebrafish. Zebrafish were kept at 28 °C and maintained at optimal breeding conditions.[36] For mating, male and female zebrafish were maintained in one tank at 28 °C on a 12-h light/12-h dark cycle, and then the spawning of eggs was triggered by giving light stimulation in the morning. Almost all eggs were fertilized immediately. All stages of zebrafish were maintained in E3 embryo media (15 mM NaCl, 0.5 mM KCl, 1 mM $MgSO_4$, 1 mM $CaCl_2$, 0.15 mM KH_2PO_4, 0.05 mM Na_2HPO_4, 0.7 mM $NaHCO_3$, 10^{-5}% methylene blue; pH 7.5). Zebrafish embryos at 19, 36, 48, and 54 hpf were incubated with 5 μM **ZTRS** in E3 media containing 0.1% (v/v) DMSO for 1 h at 28 °C.

Alternatively, 54 h-old zebrafish were exposed to 100 μM TPEN in E3 media containing 0.1% (v/v) DMSO for 1 h at 28 °C to remove intact zinc ions in zebrafish. After washing with E3 media to remove the remaining TPEN, the zebrafish were further incubated with 5 μM **ZTRS** in E3 media for 1 h at 28 °C. The treated zebrafish were imaged by fluorescence microscopy equipped with UV-2A filter.

Acknowledgment. This work was supported by the National Research Foundation of Korea (NRF) grants [20090083065, R0A-2005-000-10027-0 (NRL)], WCU programs (R31-2008-000-10010-0, R32-2008-000-10217-0), EPSRC, BBSRC, MRC, Herchel Smith Postdoctoral Research Fund and Newman Trusts.

Supporting Information Available: Fluorescence and UV−vis absorption spectra of **ZTRS** with metal ions; ^{1}H NMR, 2D NOESY, and IR spectra of **ZTRS**/Zn^{2+} and **ZTRS**/Cd^{2+} complex in CD_3CN and DMSO; X-ray crystallographic data (CIF). This material is available free of charge via the Internet at http://pubs.acs.org.

JA907334J